



OPEN

Improved β -cell function leads to improved glucose tolerance in a transgenic mouse expressing lipoprotein lipase in adipocytes

Hasiyet Memetimin^{1,3}, Beibei Zhu^{1,3}, Sangderk Lee², Wendy S. Katz², Philip A. Kern¹ & Brian S. Finlin¹✉

Lipoprotein lipase (LPL) hydrolyzes the triglyceride core of lipoproteins and also functions as a bridge, allowing for lipoprotein and cholesterol uptake. Transgenic mice expressing LPL in adipose tissue under the control of the adiponectin promoter (*AdipoQ-LPL*) have improved glucose metabolism when challenged with a high fat diet. Here, we studied the transcriptional response of the adipose tissue of these mice to acute high fat diet exposure. Gene set enrichment analysis (GSEA) provided mechanistic insight into the improved metabolic phenotype of AdipoQ-LPL mice. First, the cholesterol homeostasis pathway, which is controlled by the SREBP2 transcription factor, is repressed in gonadal adipose tissue AdipoQ-LPL mice. Furthermore, we identified SND1 as a link between SREBP2 and CCL19, an inflammatory chemokine that is reduced in AdipoQ-LPL mice. Second, GSEA identified a signature for pancreatic β -cells in adipose tissue of AdipoQ-LPL mice, an unexpected finding. We explored whether β -cell function is improved in AdipoQ-LPL mice and found that the first phase of insulin secretion is increased in mice challenged with high fat diet. In summary, we identify two different mechanisms for the improved metabolic phenotype of AdipoQ-LPL mice. One involves improved adipose tissue function and the other involves adipose tissue—pancreatic β -cell crosstalk.

Lipoprotein lipase (LPL) is highly expressed in adipose tissue and promotes the uptake of lipid for storage¹. We have developed a mouse model using the adiponectin promoter to increase LPL expression in adipose tissue². These mice (AdipoQ-LPL) have improved glucose metabolism when challenged with a high fat diet². Our initial characterization of the mouse revealed that ectopic lipids were not reduced in either liver or skeletal muscle. This was likely due to the fact that the adiponectin promoter that we utilized only increased *LPL* mRNA 1.2 fold over endogenous *LPL* levels². However, gene expression was altered in the perigonadal fat of male mice, in a manner suggesting that AdipoQ-LPL mice have less adipose dysfunction. For instance, the mRNA levels of adiponectin and other peroxisome proliferator-activated receptor (PPAR γ)-regulated genes were higher in AdipoQ-LPL mice with trends for reduced inflammatory gene expression at the end of a high fat diet induced obesity study².

Changes in adipose tissue gene expression are observed in as little as 24-h after high fat diet feeding of mice³, and these changes are thought to initiate the development of adipose dysfunction^{4,5}. One mechanism postulates that the increased hypertrophy of adipose tissue causes hypoxia and the induction of collagens which cause adipocyte death. This in turn leads to macrophage accumulation, inflammation, and adipose dysfunction⁵. Additional pathways activated by high fat feeding include endoplasmic reticulum stress; transforming growth factor- β (TGF β) and fibrosis; and sterol regulatory element-binding protein 2 (SREBP2)^{3,6,7}. Thus, identifying changes in gene expression that occur early during an acute high fat diet challenge is important for understanding mechanisms that cause the development of adipose dysfunction.

In this study, we characterize the body composition and energy expenditure of AdipoQ-LPL mice during the chow to high fat diet transition. We then identify changes in gene expression and the pathways affected in the gonadal fat of AdipoQ-LPL mice that occur early in the course of high fat diet feeding using gene set enrichment analysis (GSEA) of hallmark gene sets and other approaches. These analyses of gene expression led us to evaluate several interesting mechanisms for the improved metabolic phenotype of the AdipoQ-LPL mouse model.

¹Division of Endocrinology, and the Barnstable Brown Diabetes and Obesity Center, Department of Medicine, University of Kentucky, Lexington, KY, USA. ²Department of Pharmacology and Nutritional Sciences, University of Kentucky, Lexington, KY, USA. ³These authors contributed equally: Hasiyet Memetimin and Beibei Zhu. ✉email: bfinlin@uky.edu

Parameter	Control	AdipoQ-LPL	P
All mice before the study^a			
Weight (g)	26.4 ± 0.5	26.4 ± 0.3	0.90
Lean mass (g)	19.9 ± 0.4	19.3 ± 0.2	0.23
Fat mass (g)	2.8 ± 0.2	3.3 ± 0.2	0.04
Mice challenged with HFD^b			
Weight (g)	27.8 ± 0.6	26.4 ± 0.5	0.06
Initial lean mass (g)	20.9 ± 0.5	19.6 ± 0.4	0.03
Final lean mass (g)	20.7 ± 0.5	19.5 ± 0.3	0.03
Delta lean mass (g)	-0.2 ± 0.3	-0.1 ± 0.2	0.70
Initial fat mass (g)	3.0 ± 0.3	3.2 ± 0.3	0.62
Final fat mass (g)	7.7 ± 0.5	7.4 ± 0.4	0.61
Delta fat mass	4.7 ± 0.3	4.2 ± 0.3	0.29
Mice maintained on chow^c			
Initial weight (g)	25.2 ± 2	26.3 ± 1.6	0.13
Initial lean mass(g)	18.9 ± 1.5	19.1 ± 0.8	0.71
Final lean mass (g)	19.7 ± 1.3	19.6 ± 0.9	0.77
Delta lean mass (g)	0.8 ± 0.7	0.5 ± 0.5	0.20
Initial fat mass (g)	2.6 ± 0.5	3.5 ± 0.9	0.01
Final fat mass (g)	3.3 ± 0.8	4.6 ± 1.7	0.02
Delta fat mass (g)	0.7 ± 0.4	1.1 ± 0.9	0.12

Table 1. ECHO MRI characterization of mice. ^aAdipoQ-LPL transgenic male mice and their littermate controls (age 9–9.5 weeks) were characterized by ECHO-MRI before and after an acute high fat diet challenge in calorimetry chambers; a group of mice was maintained on chow as a control group. These data are for the entire cohort (control n = 25; AdipoQ-LPL n = 23) before the study. Data are represented as means ± standard error of the mean. ^bAdipoQ-LPL transgenic male mice and their littermate controls were characterized in a 1-week chow and 1-week high fat diet (60% cal fat) feeding study in calorimetry chambers (n = 12 control and n = 12 AdipoQ-LPL per group). Data are represented as means ± standard error of the mean. ^cAdipoQ-LPL transgenic male mice and their littermate controls were maintained on chow (n = 13 control and n = 11 AdipoQ-LPL per group). Data are represented as means ± standard error of the mean.

Results

Study design, body composition of the mice, and indirect calorimetry. The AdipoQ-LPL mouse model has improved glucose metabolism when challenged with a high fat diet². Additionally, the mice have increased food intake and increased energy expenditure after 12-weeks of high fat diet². To better understand these changes that occur after a chronic high fat diet, we characterized the initial response of the mice to high fat diet by indirect calorimetry. After a 1-week acclimation period, mice were placed in calorimetry chambers and studied for 1-week on chow and 1-week on high fat diet. Three days after the mice were removed from the calorimetry chambers (10-days total on HFD), the mice were euthanized and tissues collected for gene expression studies. An additional cohort was maintained on chow, but not characterized by microarray.

Table 1 shows the body composition of all of the mice in the study before being placed into acclimation chambers. The AdipoQ-LPL mice had a slightly higher (0.5 g) fat mass than the control mice (Table 1; $P = 0.04$); otherwise, the two groups of mice were similar. The mice were then split into two groups; one group was switched to high fat diet after 1-week in calorimetry chambers and the other was maintained on chow diet. The acute high fat diet resulted in an increase in fat mass in both groups of mice as expected (Table 1); there were no differences between the control and AdipoQ-LPL mice in weight gain, fat mass gain, or lean mass gain (Table 1). Although not statistically significant, the AdipoQ-LPL mice gained 0.4 g of fat more than the control mice over 10-days of chow feeding (Table 1; $P = 0.12$). When the calorimetry data were analyzed for the group that was switched from chow to HFD in calorimetry chambers, there were no differences between the control and AdipoQ-LPL mice in food intake, resting respiratory exchange ratio, or resting energy expenditure.

Microarray. We next performed a microarray analysis on the perigonadal fat from 12 control and 12 AdipoQ-LPL male mice from the 10-day acute high fat diet challenge. Genes with a 1.25-fold difference in expression and $P < 0.02$ are listed in Table S1. Functional annotation analysis of these genes using NIH David^{8,9} indicated that two KEGG pathways were enriched in this gene list. The steroid biosynthesis pathway was the most significantly enriched pathway ($P = 6e^{-5}$). The enzymes NAD(P) dependent steroid dehydrogenase-like (*Nsdhl*); lanosterol synthase (*Lss*); cytochrome P450 family 51 (*Cyp51*), and squalene epoxidase (*Sqle*) were the genes in the steroid biosynthesis KEGG pathway, and all four genes were lower in AdipoQ-LPL mice (Table S1). Further analysis of the gene list (Table S1) showed that two other genes involved in cholesterol homeostasis, the low density lipoprotein receptor (*Ldlr*) and insulin induced gene 1 (*Insig1*), are also repressed in AdipoQ-LPL mice. Together, these data suggest that cholesterol biosynthesis is down-regulated in the adipose of AdipoQ-LPL mice; this could be due to increased lipoprotein core uptake by the LPL, which has been demonstrated to occur in

Gene sets down in AdipoQ-LPL mice					
Name	SIZE	ES	NES	NOM P-val	FDR q-val
HALLMARK_CHOLESTEROL_HOMEOSTASIS	72	- 0.65	- 1.78	0.002	0.127
HALLMARK_UNFOLDED_PROTEIN_RESPONSE	109	- 0.42	- 1.65	0.030	0.270
HALLMARK_MTORC1_SIGNALING	185	- 0.50	- 1.59	0.042	0.281
HALLMARK_TGF_BETA_SIGNALING	54	- 0.40	- 1.46	0.085	0.417
HALLMARK_UV_RESPONSE_UP	143	- 0.29	- 1.27	0.096	0.355
HALLMARK_MYC_TARGETS_V1	175	- 0.44	- 1.58	0.100	0.235
HALLMARK_APICAL_JUNCTION	198	- 0.33	- 1.29	0.101	0.431
HALLMARK_HYPOXIA	191	- 0.32	- 1.28	0.105	0.385
HALLMARK_MYOGENESIS	195	- 0.38	- 1.28	0.106	0.413
Gene sets up in AdipoQ-LPL mice					
HALLMARK_PANCREAS_BETA_CELLS	37	0.58	1.69	0.008	0.137
HALLMARK_COAGULATION	131	0.44	1.39	0.061	0.578

Table 2. Enrichment of hallmark gene sets in adipose tissue. The microarray data for adipose tissue gene expression was analyzed by GSEA to evaluate hallmark gene sets downregulated or upregulated in AdipoQ-LPL mice. The name of the pathway, number of genes (SIZE), Enrichment and normalized enrichment scores, Nominal P values and false discovery rate q-values generated by GSEA are indicated.

other tissues^{10–16}. The PPAR signaling KEGG pathway was also detected ($P=0.05$), which was expected since we previously detected a PPAR gene signature in AdipoQ-LPL mice fed a high fat diet for 16-weeks². Phosphoenolpyruvate carboxykinase 1 (*Pck1*) was induced in AdipoQ-LPL mice (Table S1); in addition, the microarray indicated that adiponectin is induced in AdipoQ-LPL mice. The shuttle for transfer of acetyl groups from the mitochondria to the cytosol BIOCARTA pathway was detected ($P=0.05$). This pathway is involved in lipid biosynthesis, and the two genes in this pathway, malic enzyme 1 (*Me1*) and ATP citrate lyase (*Acly*), are repressed in AdipoQ-LPL mice (Table S1). In addition, Solute Carrier Family 25 Member 10 (*Slc25a10*), which is important for citrate transport from the mitochondria to the cytosol and lipogenesis¹⁷ was also repressed in AdipoQ-LPL mice (Table S1). Thus, key genes in lipid and cholesterol biosynthesis are repressed in AdipoQ-LPL mice, consistent with increased expression of LPL by the transgene.

To gain further insight into the transcriptional response of the mice, we performed gene set enrichment analysis of hallmark gene sets on all of the microarray data^{18–20}. In addition to suppression of the cholesterol homeostasis pathway, this analysis identified several pathways that contribute to adipose dysfunction are repressed in AdipoQ-LPL mice including the unfolded protein response (endoplasmic reticulum stress) and mammalian target of rapamycin complex 1 (MTORC1 signaling) (Table 2); example enrichment plots are shown in Fig. 1. The TGF β signaling and hypoxia gene sets had trends for reduction (Table 2). These pathways are upregulated early in the course of the development of adipose dysfunction by high fat feeding and are intertwined with each other. Furthermore, these pathways are linked to inflammation and fibrosis by mechanisms that are incompletely understood. An unexpected finding was the enrichment of genes involved in pancreatic β -cell development and function in the AdipoQ-LPL mice (Table 2), suggesting a possible link between adipose tissue and pancreatic β -cell function, contributing to improved glucose homeostasis. GSEA analysis thus suggested two mechanisms for the improved glucose homeostasis of the AdipoQ-LPL mice. One mechanism involves an effect on adipose tissue and the other involves adipose tissue—pancreatic β -cell cross talk.

Suppression of the cholesterol homeostasis pathway and identification of SND1 as a link between SREBP2 and inflammation in adipose tissue. Hierarchical cluster analysis indicated that SND1 was clustered with genes involved in cholesterol biosynthesis (Fig. 2), suggesting that SND1 is regulated by SREBP2. SND1 binds RNA and regulates transcription, splicing, mRNA stability, and miRNA biosynthesis. SND1 is conserved from plants to mammals, and one of its primary functions is to protect against stress by regulating cellular stress responses. As an oncogene in hepatic carcinoma, SND1 enhances inflammation and fibrosis^{21,22}, suggesting that SND1 could be an important link between SREBP2 and cellular stress responses including inflammation. Suppression of SND1 could thus contribute to the improved transcriptional response of the AdipoQ-LPL mouse.

We verified the microarray results with real time RT PCR. SND1 mRNA was repressed in perigonadal adipose tissue of AdipoQ-LPL mice (Fig. 3A; $P < 0.0001$). As shown in Fig. 3B–D, *Ldlr*, *Lss* and *Insig1*, which are SREBP2-regulated genes, were all lower in AdipoQ-LPL mice than control mice ($P < 0.05$). When we examined the *Snd1* gene structure, we found that Leucine Rich Repeat Containing 4 (*Lrrc4*) is nested in an intron of SND1 on the opposite strand²³. *Lrrc4* mRNA is higher in AdipoQ-LPL mice (Fig. 3E; $P < 0.0001$). This is the first report of the *Snd1* and *Lrrc4* genes being differentially regulated in vivo, a common phenomenon for nested genes²³. In fact, these two nested genes had by far the best two P values in this study (Table S1). Finally, although genes become nested by random, it is interesting to note that SND1 is an oncogene and *Lrrc4* is a tumor suppressor.

Because of the potential connection between SND1 and inflammation, we evaluated inflammatory gene expression. Inflammation is just beginning to develop at 10-days of high fat feeding³; therefore we did not expect to find a large number of inflammatory genes. However, in Table S1, we identified chemokine (C–C motif)

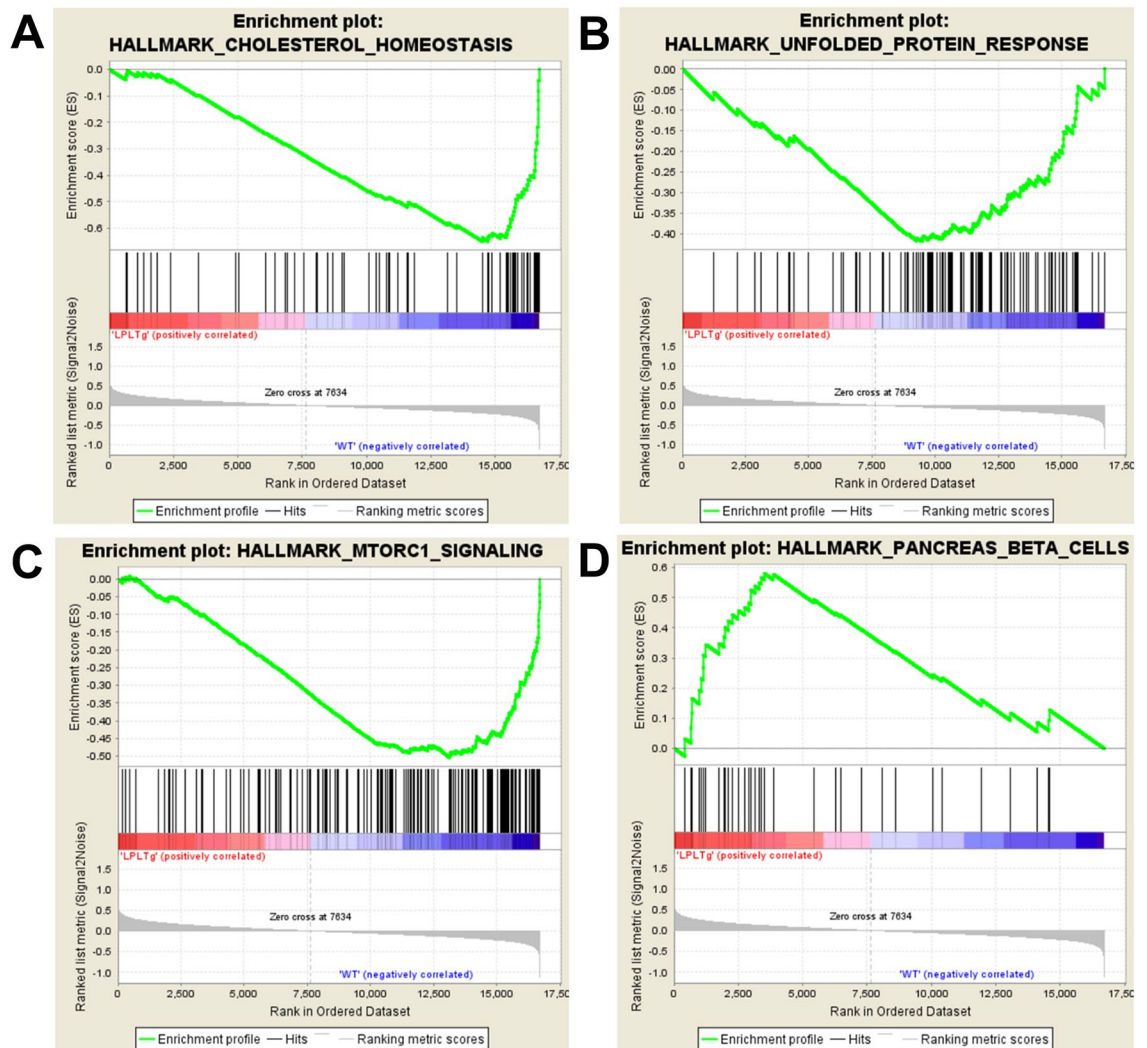


Figure 1. Enrichment plots of hallmark gene sets enriched and repressed in perigonadal adipose tissue of male AdipoQ-LPL mice. We used Affymetrix Mouse 2.0 microarrays to quantify gene expression in perigonadal adipose tissue and analyzed the entire set of data by gene set enrichment analysis to identify hallmark gene sets enriched or repressed in the AdipoQ-LPL mice ($n = 12$). (A–D) Enrichment plots for gene sets repressed and enriched in AdipoQ-LPL mice.

ligand 19 (*Ccl19*; macrophage inflammatory protein 3b), a chemokine for dendritic cells, which promote adipose inflammation²⁴, and confirmed that it was repressed in AdipoQ-LPL mice (Fig. 3F; $P < 0.05$).

SND1 mRNA and protein expression and regulation in adipocytes. To identify cell types where *Snd1* is expressed in adipose tissue and regulated by LPL, we collagenase digested adipose tissue and measured *Snd1* in the floating adipocytes. *Snd1* mRNA was significantly repressed in the AdipoQ-LPL mouse floating adipocytes (Fig. 4A; $P < 0.05$). *Snd1* was expressed in the stromal vascular fraction, and there was a trend for lower expression in the AdipoQ-LPL mice ($P = 0.07$; not shown). Next, we confirmed that SND1 protein levels were reduced in floating adipocytes from the AdipoQ-LPL mouse (Fig. 4B; $P < 0.05$; images of the uncropped gels are in supplemental Fig. 1). Finally, we characterized *Snd1* mRNA expression during a time course of differentiation of 3T3-L1 cells into adipocytes. *Adiponectin* expression was low in preadipocytes and increased during the time course of differentiation as expected. *Snd1* mRNA was expressed during all stages of differentiation (Fig. 4C) as previously observed²⁵. Thus, *Snd1* is expressed in adipocytes, reduced in AdipoQ-LPL mice, and 3T3-L1 adipocytes are a suitable model for in vitro studies of SND1.

Since *Snd1* clustered with genes in the cholesterol homeostasis pathway, we determined the effects of cholesterol depletion and reduction of SREBP2 by siRNA on *Snd1* mRNA expression in adipocytes. We treated differentiated 3T3-L1 adipocytes with lipoprotein deficient serum (LPDS) containing compactin and a low level of mevalonate to prevent toxicity; cholesterol was added to the same media to inhibit SREBP2. Addition of cholesterol to the media repressed *Ldlr* mRNA expression as expected, and *Snd1* mRNA expression was also repressed (Fig. 5A,B; $P < 0.001$), suggesting that SREBP2 positively regulates SND1 expression in adipocytes. Next, we used siRNA to reduce SREBP2 in differentiated 3T3L1 cells. Treatment of 3T3L1 cells with SREBP2

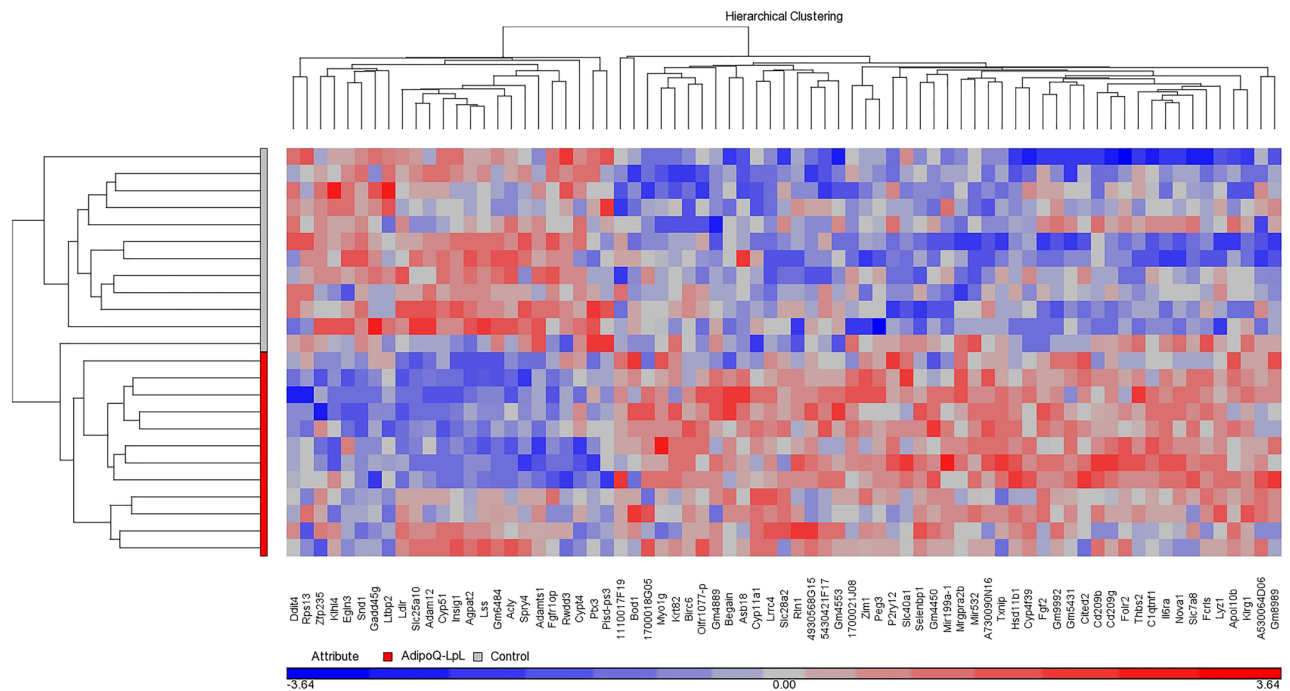


Figure 2. Hierarchical clustering of gene expression. The heat map was generated with Partek using genes with a P value less than 0.01 and a 1.25-fold change in expression.

siRNA reduced SREBP2 mRNA levels (Fig. 5C; $P < 0.01$) and SREBP2 protein (mature) levels (Fig. 5D; $P < 0.05$; images of the uncropped gels are in supplemental Fig. 2). We note that we did not detect the parental form of SREBP2 likely due to the use of serum free medium in this experiment (see full blots in supplemental Fig. 2). Reducing SREBP2 with siRNA reduced SND1 mRNA levels (Fig. 5E; $P < 0.05$).

SND1 promotes inflammatory cytokine and chemokine expression in adipocytes. SREBP2 promotes inflammation, but the precise mechanism is not known. SND1 promotes nuclear factor kappa-light-chain-enhancer of activated B cells (NF κ B) activity in hepatic carcinoma²², and could thus be a link between SREBP2 and inflammation in adipocytes. Since activation of the NF κ B pathway has been strongly implicated in the development of adipose inflammation^{26,27}, we determined whether reducing SND1 expression would inhibit the induction of inflammatory cytokines that are known to be regulated by NF κ B in differentiated 3T3-L1 adipocytes. We also evaluated *Ccl19* since it is an inflammatory chemokine^{24,28} that was repressed 1.4-fold in AdipoQ-LPL mice (Table S1; $P = 0.013$), which was confirmed by real time RT PCR (Fig. 3F; $P < 0.05$). We treated 3T3-L1 adipocytes with control (scramble) siRNA or SND1 siRNA and 48-h later treated them with tumor necrosis factor- α (TNF α) to induce an inflammatory response. Treatment of differentiated 3T3L1 cells with SND1 siRNA significantly reduced SND1 mRNA and protein levels (Fig. 6A,B; $P < 0.05$; images of the uncropped gels are in supplemental Fig. 3). Next, we determined whether lowering SND1 with siRNA would reduce inflammatory gene expression in response to TNF α treatment. Interleukin 6 (*IL6*) and monocyte chemoattractant protein 1 (*MCP1*) were evaluated as classical inflammatory genes, and *Ccl19* was evaluated because it was shown to be lower in adipose tissue of AdipoQ-LpL mice and is also an inflammatory gene. *Ccl19*, *IL6*, and *MCP1* were induced by TNF α and repressed in *Snd1* siRNA in 3T3-L1 adipocytes (Fig. 6B–D; $P < 0.05$).

SND1 regulates *Ccl19* splicing. SND1 regulates mRNA splicing by promoting the inclusion of exons with weak splice sites²⁹; therefore, we analyzed the array data for gene splicing. This revealed a significant number of genes with alternative splicing (Table S2) including *Ccl19*. The *Ccl19* gene has 4 exons; the microarray revealed that exons 2 and 3 of *Ccl19* are reduced in AdipoQ-LPL mice, suggesting that shorter isoforms exist. We designed PCR primers in exons 1 and 4 that would generate distinct PCR products if exons 2 or 3 are not in *Snd1* mRNA in adipose tissue, and RT PCR using these two primers on the adipose tissue of control and AdipoQ-LPL mice revealed that two isoforms exist (Fig. 7A). Sequence analysis of the PCR products revealed the presence of two distinct isoforms: full length *Ccl19* and the short isoform, which is composed of exons 1, 3, and 4 (we note an anomaly in the way the gel ran affecting the migration of the isoforms in lane 5). We quantified the gel and found that *Ccl19* (exons 1,3,4) was more abundant in the adipose tissue of AdipoQ-LPL mice, and the full length form was more abundant in control mice, consistent with the microarray (Fig. 7B; $P < 0.01$). The exon structure and alternate splicing of *Ccl19* is shown in Fig. 7C. The *Ccl19* (1,3,4) splice isoform shifts the reading frame and causes a premature stop codon in the signal sequence such that no part of the secreted protein is made (Fig. 7D). Thus, the alternative isoform is completely inactive, and the regulation of *Ccl19* splicing is an effective mechanism for controlling *Ccl19* protein expression.

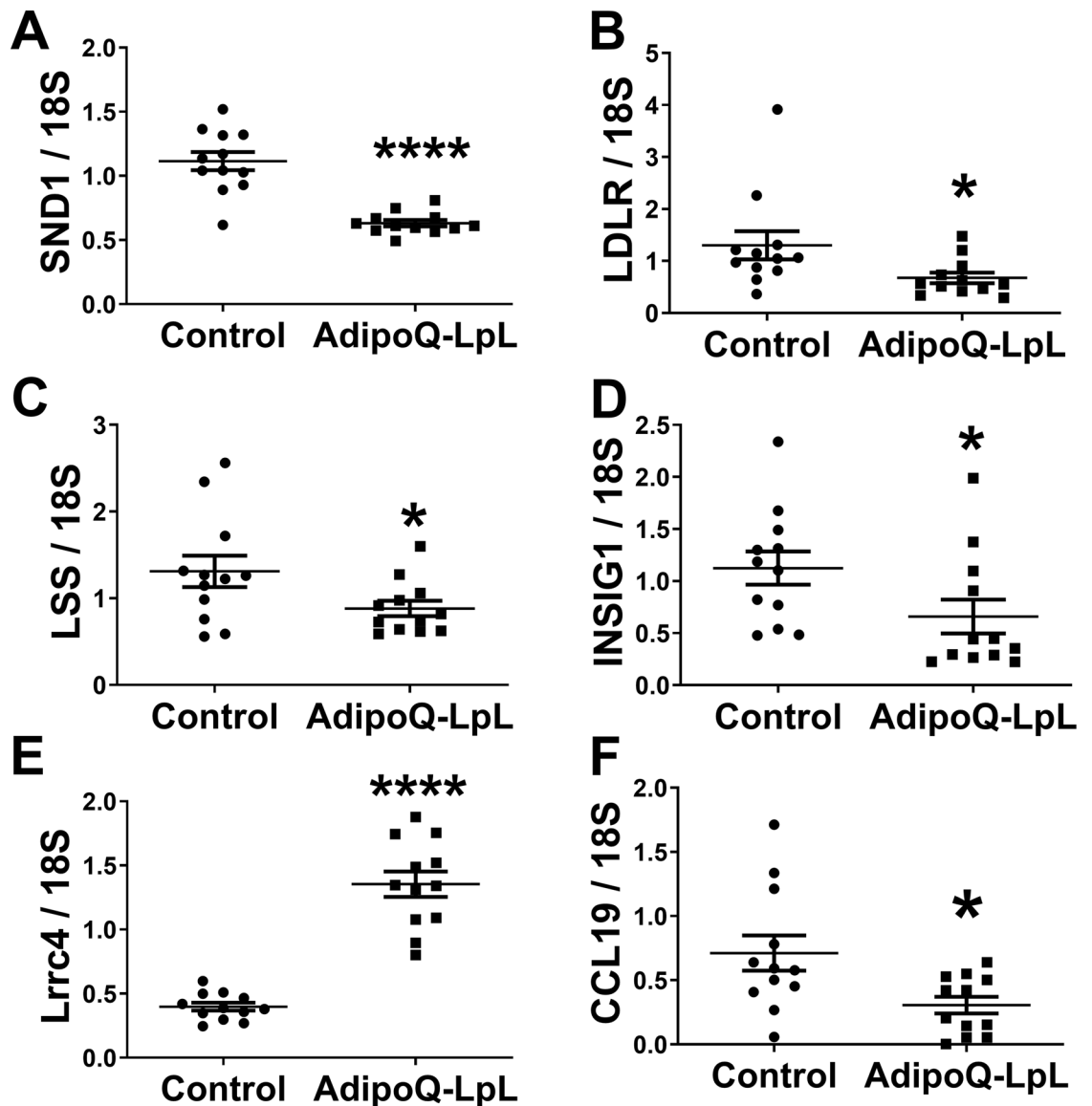


Figure 3. Confirmation of the microarray results. mRNA expression in perigonadal fat of control and AdipoQ-LpL mice on chow or high fat diet (10-days) was measured by real-time RT-PCR. The data are represented as the mean \pm SEM of gene expression normalized to 18S (n = 12). mRNA expression of (A) SND1, (B) LDLR, (C) LSS, (D) INSIG1, (E) *Lrrc4*, and (F) *Ccl19* is indicated (*P < 0.05; ****P < 0.0001; two-tailed unpaired Student's t-test). Data for *Ccl19* is log10 transformed.

To determine whether SND1 regulates *Ccl19* splicing, we evaluated control and *Snd1* siRNA treated adipocytes that were induced to express *Ccl19* by TNF α treatment in Fig. 6. PCR analysis indicated that TNF α -treatment induced two *Ccl19* isoforms (Fig. 7E inset). We then determined the expression level of each exon with exon specific primers, using *Ccl19* plasmid DNA to generate the standard curve, and determined the ratio of each exon to exon 1. As shown in Fig. 7E, the ratio of exon 2 to exon 1 was significantly decreased by *Snd1* siRNA (P < 0.05); *Snd1* siRNA treatment did not significantly reduce the exon 3 to exon 1 or the exon 4 to exon 1 ratios. Thus, SND1 promotes the inclusion of exon 2 into *Ccl19*, suggesting that reduced SND1 in vivo is responsible for the differential splicing of *Ccl19* observed in vivo (Fig. 7A,B). An analogous function has recently been shown for SND1 in cancer since it promotes the generation of splice isoforms of *CD44* that are oncogenic²⁹.

Metabolic phenotyping and insulin secretion. AdipoQ-LpL mice have improved glucose tolerance; however, the mechanism(s) are not completely identified³⁰. An unexpected finding of the GSEA analysis of the microarray was the enrichment of the pancreatic β -cell hallmark gene set (shown in Table 3) in adipose tissue of AdipoQ-LpL mice (Table 2). Hyperglycemia has been demonstrated to cause low levels of insulin expression in extra pancreatic tissues including adipose and liver tissues^{31,32}. We therefore performed immunohistochemistry on the adipose tissue from the male mice on 10 days HFD that were characterized by micro array with insulin and pdx-1 antibodies, but were unable to identify insulin positive cells (not shown) and did not further char-

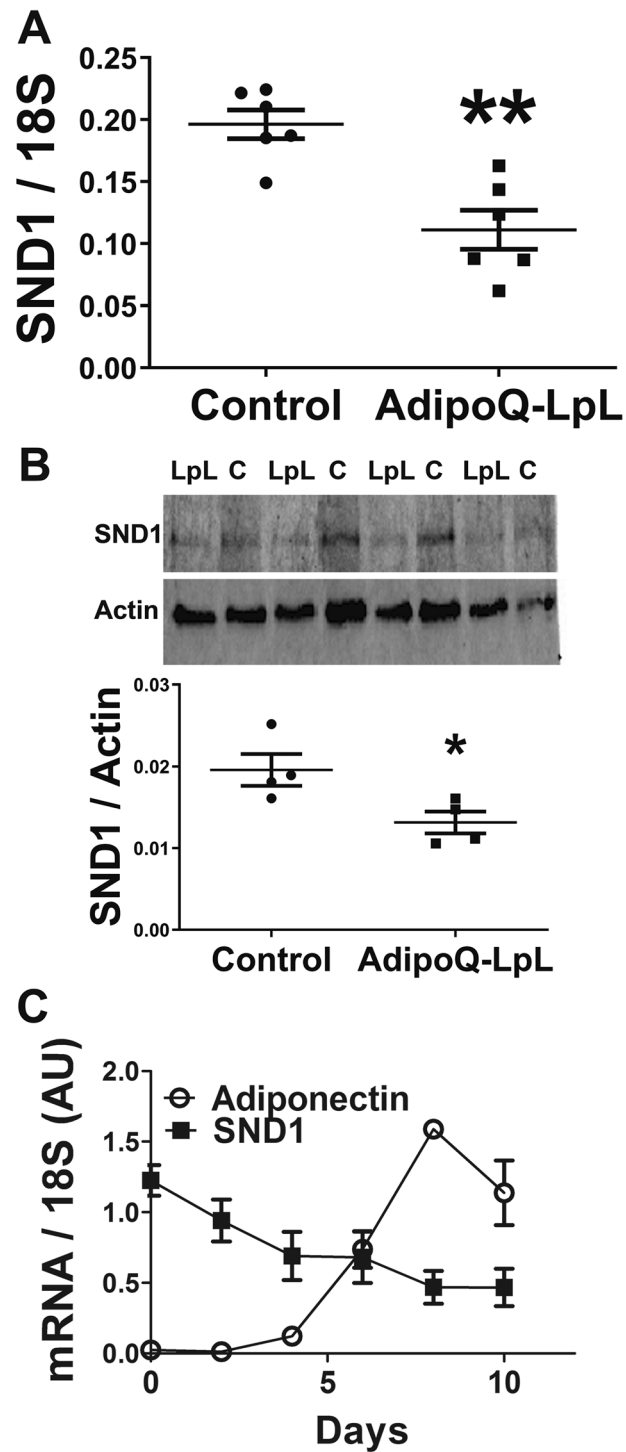


Figure 4. SND1 mRNA and protein expression in adipocytes. **(A)** SND1 mRNA expression was measured in the floating adipocytes obtained by collagenase digestion of adipose tissue from control and AdipoQ-LPL mice high fat diet (10-days). The data are represented as the mean \pm SEM ($n = 6$; $**P < 0.01$; two-tailed unpaired Student's *t*-test). **(B)** SND1 and actin were immunoblotted in lysates of floating adipocytes from control (C) and AdipoQ-LPL (LpL) mice on the high fat diet (10-days). The ratio of SND1 to actin was calculated, and the data are represented as the mean \pm SEM ($n = 4$; $*P < 0.05$; two-tailed unpaired Student's *t*-test). **(C)** *Snd1* or *AdipoQ* mRNA expression during a time course of 3T3-L1 adipocyte differentiation ($n = 3$).

acterize adipose tissue for the presence of β -cells by measuring gene expression of genes in the GSEA gene set (Table 3). Adipose tissue contains mesenchymal stem cells that can be induced to differentiate into pancreatic β -cells *in vitro*³¹, and it is possible that increased LPL expression can stimulate a pancreatic β -cell gene signature

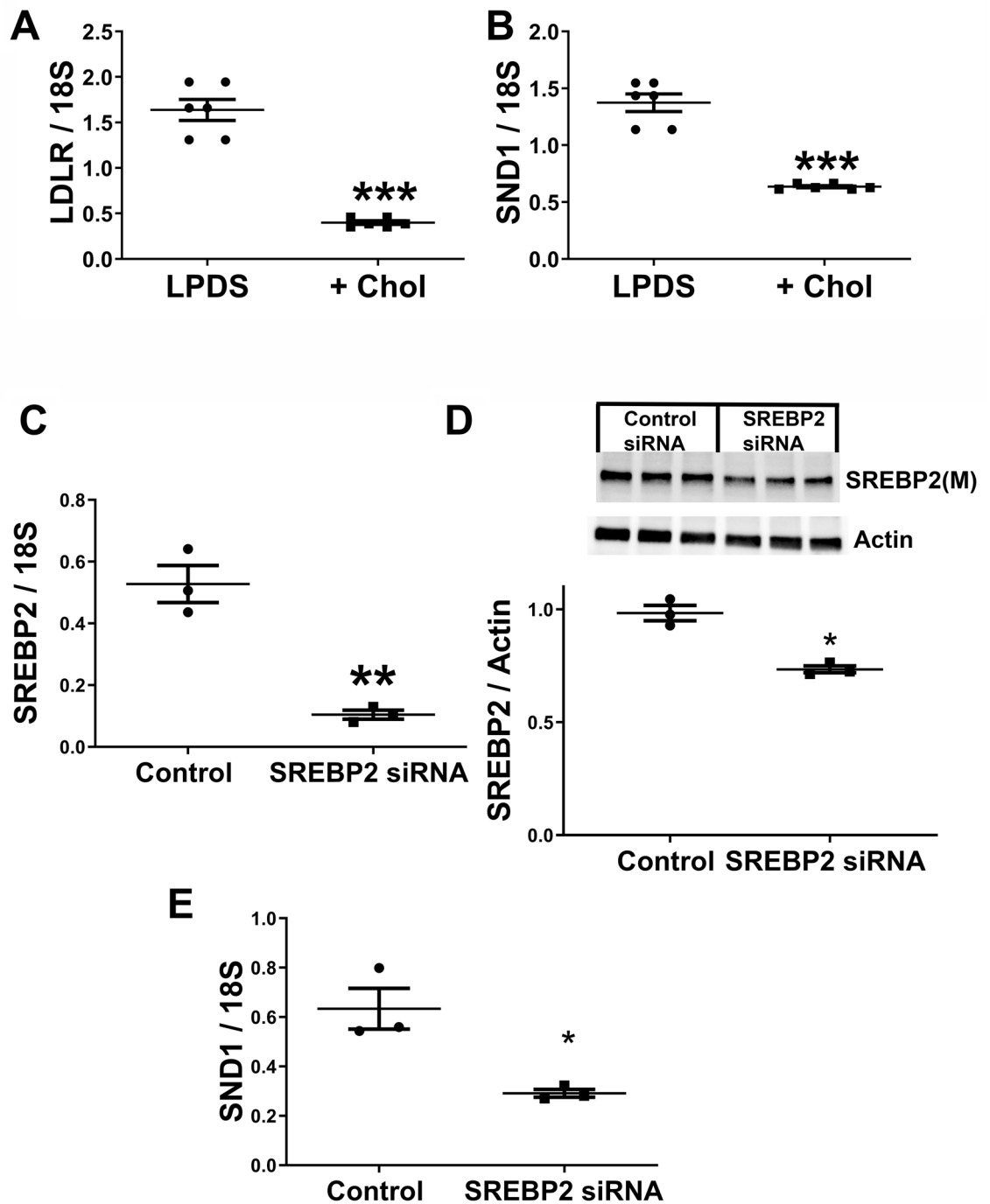


Figure 5. SREBP2 regulates *Snd1* mRNA expression. (A,B) Differentiated 3T3-L1 adipocytes were treated with lipoprotein deficient serum containing media (LPDS) for 24-h. The cells were then incubated in LPDS or LPDS with cholesterol (Chol) as indicated. Real-time RT-PCR was used to measure the gene expression of *Ldlr* and *Snd1*. Next, differentiated 3T3-L1 adipocytes were treated with control (scrambled) or SREBP2 siRNA. (C) SREBP2 mRNA expression was measured. (D) SREBP2 (M:mature form) and actin were immunoblotted and quantified. (E) *SND1* mRNA expression was determined. The data are represented as the mean \pm SEM (n=6 (A and B) or n=3 (C–E); *P<0.05; **P<0.01; ***P<0.001 two-tailed unpaired Student's t-test).

in these cells in adipose tissue. We hypothesized that if increased LPL in adipocytes of adipose tissue causes the secretion of factors that directs adipose mesenchymal stem cells towards a β -cell phenotype, then these factors could be released into the circulation to influence β -cell function in the pancreas. We therefore characterized glucose stimulated insulin secretion in AdipoQ-LPL mice to determine whether adipose tissue— β -cell crosstalk is a mechanism for the improved glucose tolerance of this mouse model.

We previously observed that if we place 5 week old AdipoQ-LPL mice on a high fat diet for 16 weeks, they have improved glucose and insulin tolerance². However, in that model, the improved insulin sensitivity of the

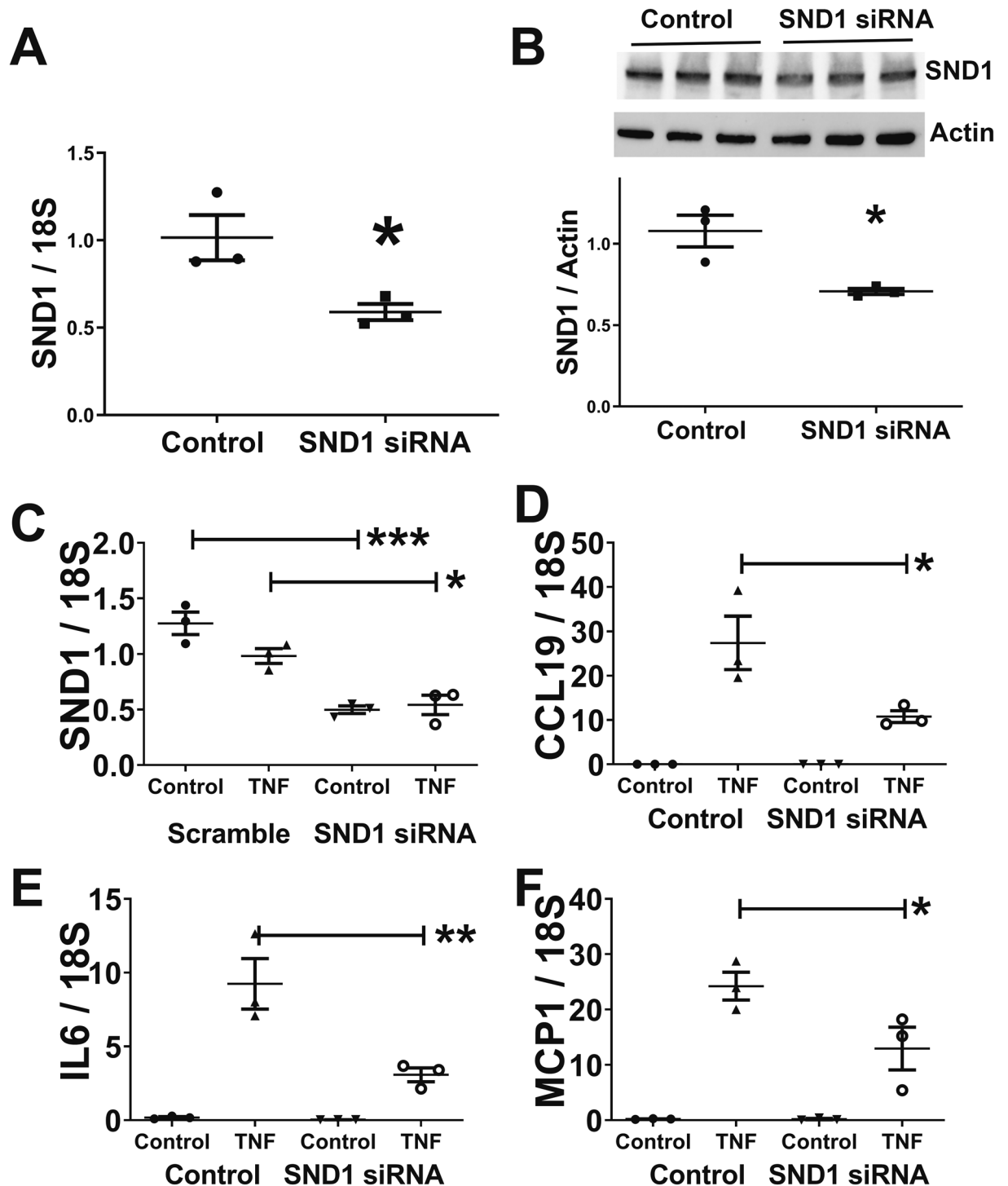


Figure 6. Snd1 promotes inflammatory gene expression in adipocytes. (A,B) Differentiated 3T3-L1 adipocytes were treated with control (scrambled) or *Snd1* siRNA as indicated, and *Snd1* mRNA expression and protein expression were determined. (C–F) Differentiated 3T3-L1 adipocytes were treated with control or *Snd1* siRNA as indicated. Next, they were treated with 20 ng/mL TNF α for 6-h. The mRNA expression of (C) Snd1, (D) CCL19, (E) IL6, and (F) MCP1 was determined with real time RT-PCR. The data are represented as the mean \pm SEM (n = 3; *P < 0.05; **P < 0.01; ***P < 0.001; one way ANOVA with Tukey post hoc test); the data for Snd1 is log transformed.

mice confounds studying insulin secretion. In a slightly different model, we have observed that if we place 8 week old AdipoQ-LPL mice on high fat diet for 18 weeks, they gain about 15 g more weight than 5 week old mice placed on HFD for 16 weeks (the original model²). The weights of mice maintained on chow or placed on

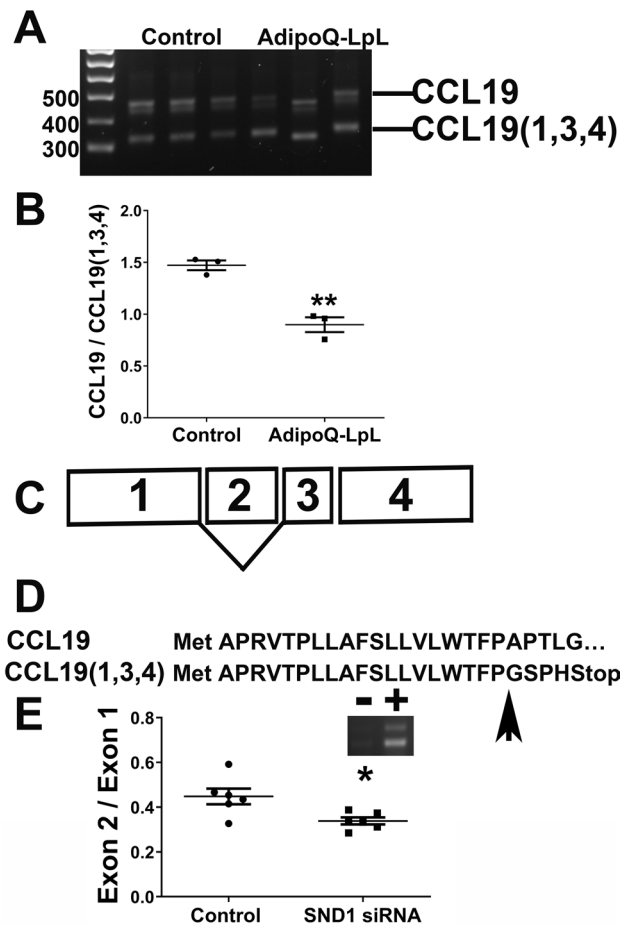


Figure 7. SND1 regulates *Ccl19* splicing. (A) RNA from the adipose tissue of control or AdipoQ-LPL mice was subjected to PCR with primers located in exon 1 and 4 of *Ccl19*. The PCR products were resolved on an agarose gel and then sequenced. The positions of full-length *Ccl19* and the shorter isoform, which was found to lack exon 2 by DNA sequencing, are indicated. (B) The ratio of full-length *Ccl19* to *Ccl19* (1,3,4) was calculated. The data are represented as the mean \pm SEM (n = 3; **P < 0.01; two-tailed unpaired Student's t-test). (C) A diagram showing the four exons of *Ccl19* and alternative usage of exon 2. (D) Translation of the full-length and *Ccl19* (1,3,4) reveals that when exon 2 is missing, the reading frame shifts and a premature stop codon is present. The arrow indicates the position of the amino acid affected by the frame shift. (E) Inset: induction of two *Ccl19* isoforms in 3T3-L1 adipocytes by TNF α . The ratio of exon 2 to exon 1 in 3T3-L1 adipocytes treated with scrambled or *Snd1* siRNA and the TNF α were calculated by real time RT-PCR with exon specific primers and *Ccl19* plasmid DNA to construct the standard curve. The data are represented as the mean \pm SEM (n = 6; *P < 0.05; two-tailed unpaired Student's t-test).

HFD at 8 weeks are shown in Fig. 8A (we note that two cohorts of mice on HFD were studied; one cohort was characterized for glucose and insulin tolerance, and the second cohort was characterized for insulin secretion; the data shown is for both cohorts combined). AdipoQ-LPL mice that were placed on HFD for 16 weeks starting at 8 weeks of age do not have improved insulin sensitivity (Fig. 8B; P = 0.41), but still have improved glucose tolerance (Fig. 8C; P = 0.026). The results in Fig. 8C were also significant when area under the curve was analyzed (Fig. 8C inset). There was no improvement of glucose tolerance in AdipoQ-LPL mice on chow diet (Fig. 8D). Therefore, we studied insulin secretion during a glucose challenge in this mouse model since increased insulin secretion would explain the improvement in glucose tolerance. After 16 weeks on chow, there was no significant difference in insulin secretion (P = 0.13) between genotypes (Fig. 8E). At 16 weeks on HFD, the AdipoQ-LPL mice demonstrated increased insulin secretion (interaction P = 0.017), and this was due to an increase first phase insulin secretion (P < 0.01), which occurred 2 min after glucose injection (Fig. 8F).

Summary and conclusion. Analyzing the adipose tissue transcriptional response to acute HFD challenge revealed two interesting mechanisms for the improved glucose homeostasis of LPL mice. First, SREBP2 is repressed in adipose tissue, and we found that SND1 is regulated by SREBP2. Thus SND1 is an important link between SREBP2 and inflammatory responses. Second, pancreatic β -cell function is improved in AdipoQ-LPL mice since first phase insulin secretion is improved when diet induced obese mice are challenged with glucose.

Gene symbol ^a	Gene title
SYT13	Synaptotagmin XIII
MAFB	v-maf musculoaponeurotic fibrosarcoma oncogene homolog B (avian)
INSM1	Insulinoma-associated 1
INS	Insulin
PCSK1	Proprotein convertase subtilisin/kexin type 1
NKX6-1	NK6 transcription factor related, locus 1 (Drosophila)
DCX	Doublecortex; lissencephaly, X-linked (doublecortin)
CHGA	Chromogranin A (parathyroid secretory protein 1)
NEUROD1	Neurogenic differentiation 1
SLC2A2	Solute carrier family 2 (facilitated glucose transporter), member 2
SCGN	Secretagoin, EF-hand calcium binding protein
SST	Somatostatin
G6PC2	Glucose-6-phosphatase, catalytic, 2
FOXA2	Forkhead box A2
AKT3	v-akt murine thymoma viral oncogene homolog 3 (protein kinase B, gamma)
null	Null
GCK	Glucokinase (hexokinase 4, maturity onset diabetes of the young 2)
DPP4	Dipeptidyl-peptidase 4 (CD26, adenosine deaminase complexing protein 2)
PCSK2	Proprotein convertase subtilisin/kexin type 2
PAX4	Paired box gene 4
ISL1	ISL1 transcription factor, LIM/homeodomain, (islet-1)
GCG	Glucagon
ABCC8	ATP-binding cassette, sub-family C (CFTR/MRP), member 8
null	Null
PAX6	Paired box gene 6 (aniridia, keratitis)
null	Null
NKX2-2	NK2 transcription factor related, locus 2 (Drosophila)
IAPP	Islet amyloid polypeptide
PAK3	p21 (CDKN1A)-activated kinase 3
VDR	Vitamin D (1,25-dihydroxyvitamin D3) receptor
NEUROG3	Neurogenin 3
SPCS1	Signal peptidase complex subunit 1 homolog (S. cerevisiae)
LMO2	LIM domain only 2 (rhombotin-like 1)
STXBP1	syntaxin binding protein 1
PKLR	Pyruvate kinase, liver and RBC
SRP9	Signal recognition particle 9 kDa
SRPRB	Signal recognition particle receptor, B subunit

Table 3. Genes in the pancreatic β -cell gene set. ^aThe gene symbols and gene titles of the GSEA pancreatic β -cell gene set are indicated.

This represents an important example of adipose tissue—pancreatic β -cell cross talk and provides a direct mechanism for the improved glucose tolerance of the AdipoQ-LPL mice.

Discussion

We have characterized physiological responses and adipose tissue transcriptional responses of AdipoQ-LPL mice to a 10-day high fat diet challenge. Although, the AdipoQ-LPL mouse has increased food intake and increased resting energy expenditure after long term HFD², no phenotype was apparent during the switch from chow to HFD in our calorimetry experiments. We characterized the transcriptional response to HFD in perigonadal adipose tissue since we observed significant changes in gene expression in that depot after long term HFD². This analysis identified two interesting mechanisms by which increasing adipose tissue LPL reduces adipose dysfunction and improves glucose homeostasis. One mechanism involves the repression of the SREBP2 pathway, and further molecular analysis revealed that SND1 is induced by this pathway in gonadal adipose tissue, and that SND1 regulates CCL19 and promotes inflammatory cytokine production in vitro. The second mechanism involves improved pancreatic β -cell function. AdipoQ-LPL challenged with a high fat diet have increased first phase insulin secretion, which improves glucose tolerance.

A prominent aspect of the transcriptional response of AdipoQ-LPL mice is to repress enzymes involved in lipogenesis and cholesterol biosynthesis, which is a predicted response to increasing lipoprotein triglyceride

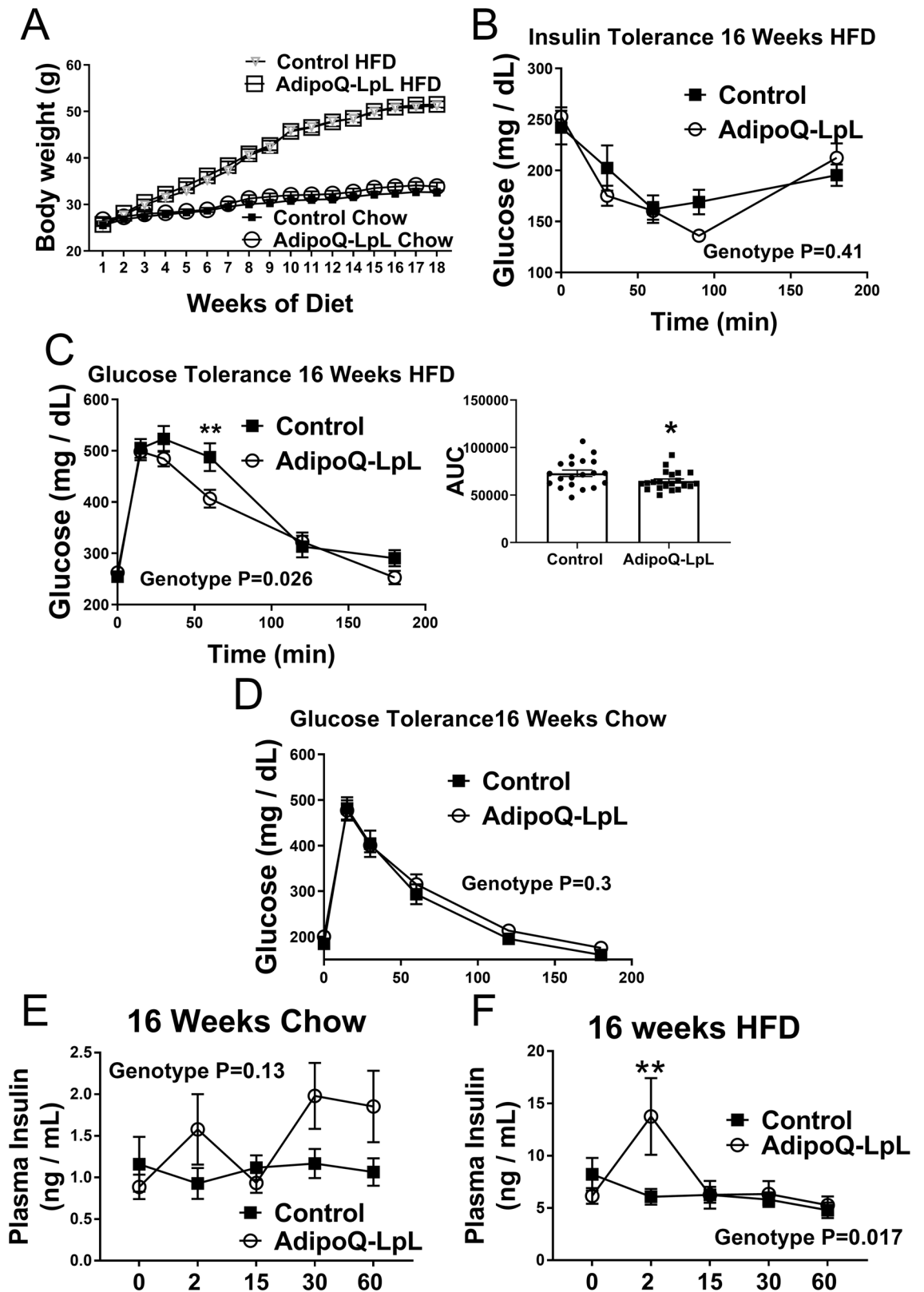


Figure 8. Glucose homeostasis and insulin secretion of control and AdipoQ-LpL mice. (A) Weight of the mice after switching to HFD (control n = 20; AdipoQ-LpL n = 21) or maintaining on chow (n = 12) starting at 8-weeks. (B) Glucose tolerance of control and AdipoQ-LpL mice after 16 weeks of HFD (control n = 20; AdipoQ-LpL n = 21). (C) Insulin tolerance of control and AdipoQ-LpL mice after 16 weeks of HFD (control n = 9; AdipoQ-LpL n = 9). Inset: analysis of area under the curve. (E,F) Plasma insulin levels after glucose injection of control and AdipoQ-LpL mice after chow or HFD for 16 weeks (control n = 11; AdipoQ-LpL n = 12; both cohorts 2 min glucose n = 6). Data were analyzed by RM 2 way ANOVA **P < 0.01; interaction P values for genotype are indicated in the figure.

hydrolysis and core uptake. We also found that genes regulated by PPAR γ are upregulated in AdipoQ-LPL mice, which is also expected. In addition to this, GSEA revealed that several pathways thought to contribute to adipose dysfunction are repressed in AdipoQ-LPL mice. The primary mechanism likely involves increased lipoprotein core uptake into adipose and suppression of SREBP2 activity. SREBP2 is activated in adipocytes by high fat feeding to supply cholesterol for the growing plasma membrane and lipid droplet^{6,33,34}. SREBP2 activation induces inflammatory cytokine expression during this process and others^{6,35}, but the mechanisms are not completely understood. In this study, we find that the RNA binding protein SND1 is regulated by SREBP2 and contributes to inflammatory cytokine induction. It is likely that the down-regulation of SREBP2 in the adipose tissue of AdipoQ-LPL mice is a major contributor to the reduction in *Snd1* expression since our in vitro studies in 3T3L1 cells demonstrated that *Snd1* is regulated by SREBP2. Indeed, a recent study showed that human SND1 is regulated by SREBP2³⁶. Other pathways may also repress *Snd1* in AdipoQ-LPL mice since *Snd1* is also regulated by ER stress³⁷, which GSEA indicated was down regulated in AdipoQ-LPL mice. *Snd1* is regulated by NF κ B^{38,39}, but we found that treatment of differentiated 3T3-L1 adipocytes with TNF α did not increase *Snd1* expression; the mechanism for this is unclear, but should be investigated in future studies.

SND1 is highly conserved and protects organisms from plants to eukaryotic cells from stress by its ability to interact with RNA and proteins⁴⁰. By binding RNA, SND1 regulates mRNA expression at many levels including transcriptional coactivation, gene splicing, mRNA stability, and miRNA processing. SND1 is thus an interesting target of SREBP2 for a number of reasons. Studies in which SND1 is manipulated indicate that SND1 regulates the expression of genes involved in lipid biogenesis^{41–44} and very low density lipoprotein secretion in the liver⁴⁵. Thus, SND1 may provide additional transcriptional regulation of genes involved in cholesterol biogenesis in response to SREBP2 activation, for example by regulating transcriptional activation and splicing. We found that SND1 regulates the splicing of *Ccl19*; however, a number of genes are alternatively spliced in AdipoQ-LPL mice (Table S2), and it will be interesting to examine the role of SND1 in this process. In addition, SND1 is a transcriptional cofactor for PPAR γ and other transcription factors that are important in adipocytes. We did not observe repression of PPAR γ regulated genes in response to reduced SND1. This could be due to stimulation of PPAR γ by fatty acids generated by LPL; indeed, *Pck1* is induced in AdipoQ-LPL mice (Table S2).

In addition to regulating lipid biosynthesis SREBPs regulate immune responses^{46,47}, and an example of this is the induction of TNF α and IL6 in adipocytes⁶, which is thought to be mediated by NF κ B activation since these genes do not contain sterol response elements. Thus, the mechanisms by which SREBPs promote NF κ B activation are unclear. We find that SND1 is induced by SREBP2 activation, and SND1 increases MCP1 and IL6 in TNF α -stimulated adipocytes, consistent with its ability to promote NF κ B activity in hepatocytes²².

Our analysis of the microarray data uncovered an additional mechanism by which SND1 promotes inflammation: regulation of *Ccl19* alternative splicing. CCL19 is induced early in response to HFD challenge in adipose tissue²⁴. Two studies suggest that mice deficient in the CCL19 receptor C–C motif chemokine receptor 7 (CCR7) are protected against diet induced obesity, adipose inflammation, and insulin resistance^{24,48}; however, another study found no difference of CCR7 deficiency on metabolic homeostasis⁴⁹. Here, we find that *Ccl19* is regulated by alternative splicing in vivo in AdipoQ-LPL mice, and our investigation of the mechanism in vitro revealed that SND1 promotes the inclusion of exon 2 into *Ccl19* mRNA. Similar to this, SND1 has recently been shown to promote the inclusion of an exon with a weak splice site into *Cd44* to promote tumorigenesis²⁹. Thus, regulation of alternative splicing is an important function of SND1, and it will be interesting to investigate the alternative splicing of other genes that we have identified in this study including metabolic genes and genes involved in adipose dysfunction.

An unexpected finding from the GSEA analysis was the identification of the pancreatic β -cell hallmark in gonadal adipose tissue. The mRNA level of insulin was very low in adipose tissue, and it was thus unlikely that insulin secretion from adipose tissue, if any, was having an impact on glucose homeostasis in the AdipoQ-LpL mouse. We did not pursue the mechanism by which increasing LPL in adipocytes results in the pancreatic β -cell hallmark in gonadal adipose tissue. We propose that increased adipocyte LPL was increasing the expression level of protein factors or affecting lipid or metabolite levels that affect mesenchymal stem cell differentiation pathways. For instance, betacellulin was identified in Table S1, and it is known that betacellulin stimulates the formation of insulin secreting cells⁵⁰. We propose a similar model for adipose tissue—pancreatic beta cell crosstalk where increased LPL expression in adipocytes causes the release of proteins, bioactive lipids, or other factor that affect β -cell function in the pancreas. Thus an important goal is to identify these factors and determine their effects in vivo and on islets ex vivo. Our studies on insulin secretion revealed that AdipoQ-LPL mice have increased first phase insulin secretion. It is interesting that only first phase insulin secretion was affected. There are thought to be two pools of insulin granules, a reserve pool and a readily releasable pool⁵¹, and it will be important to dissect the mechanism by which first phase insulin secretion is increased in the AdipoQ-LPL mouse model.

We initially hypothesized that increasing expression of LPL in adipocytes would reduce lipotoxicity and improve insulin sensitivity and glucose homeostasis. However skeletal muscle and liver did not have reduced diacylglycerol or ceramide when the AdipoQ-LPL mice were placed on HFD, and this is likely due to the fact that the adiponectin promoter only modestly increases adipose tissue LPL mRNA levels². We did not isolate pancreatic islets in this study, and it is possible that there is reduced pancreatic β -cell lipotoxicity, which would improve β -cell function^{52–54}. Other mechanisms possible for enhanced β -cell function would be that proteins are secreted from adipose tissue that affect β -cell function. Cross talk between adipose tissue and the pancreas has recently begun to be explored. Adiponectin and leptin both have positive effects on pancreatic β -cells by reducing lipotoxicity, and adipisin has been recently demonstrated to have positive effects on β -cells and insulin secretion^{55,56}. It is thus possible that AdipoQ-LPL mice increase these or other factors such as lipids or metabolites that, in turn, affect β -cell function in the setting of HFD-induced obesity. Indeed, we previously observed increased adiponectin in the serum of AdipoQ-LPL mice³⁰. Identification of the molecules mediating adipose tissue- β -cell crosstalk in this mouse model is an important future goal.

There are important limitations to this study. First, the microarray used was not as comprehensive as RNA seq, and thus certain genes and pathways may be over or under represented. Second, analysis of the microarray data by GSEA indicated enrichment of a β -cell hallmark in the adipose tissue of the AdipoQ-LPL mice. However, we were not able to confirm the presence of beta cells in adipose tissue, and the source of this signal is unknown. We utilized the GSEA result only to hypothesize adipose tissue—beta cell cross talk. This hypothesis relies on the tissue specific expression of LPL by the adiponectin promoter. We have not observed transgene expression in tissues besides adipose² as expected, but have not tested all tissues and cell types.

In conclusion, analyzing the transcriptional response of AdipoQ-LPL mice has revealed that several pathways that contribute to adipose tissue dysfunction are repressed including the SREBP2 pathway. *Snd1* gene and protein expression are increased by SREBP2 activation, and SND1 promotes inflammatory cytokine and chemokine expression, including regulating the expression of the active *Ccl19* splice isoform. SND1 may be an important SREBP2 target due to SND1's ability to control transcriptional responses at multiple levels. Finally, this study suggests that increasing LPL in adipose tissue may stimulate signaling pathways between adipose tissue and pancreatic β -cells, which could have a significant impact on glucose homeostasis.

Materials and methods

Animal studies. All of the studies involving mice were approved by the University of Kentucky Institutional Animal Care and Use Committee. The mice were housed and given high fat diet (HFD) (60% kcal from fat; D12492; Research Diets, New Brunswick, NJ, USA) at the indicated age as previously described². Body composition was determined before and after the indirect calorimetry study with an Echo MRI system (Echo Medical Systems, Houston, TX, USA). Mice were evaluated by indirect calorimetry (TSE systems, Chesterfield, MO, USA). Wild-type female C57B6/J mice (The Jackson Laboratory, Bar Harbor, ME, USA) were used for back-crossing. Euthanasia was performed on conscious mice using carbon dioxide. All methods were performed in accordance with relevant guidelines and regulations. The study is reported in accordance with ARRIVE guidelines.

Cell culture and treatments. 3T3-L1 cells (ATCC) were cultured in DMEM (Life technologies, Grandland, NY, USA) with 10% new born calf serum (TCB, Tulare, CA, USA) and differentiated into adipocytes as follows. Cells were seeded at density of 8×10^4 /well in 6-well plates, and the medium was changed every day until they became confluent. 48-h after becoming confluent, the medium was replaced with differentiation medium (DMEM with 10% FBS (TCB, Tulare, CA, USA), 1 μ M dexamethasone (Sigma, St. Louis, MO, USA), 0.5 mM methylisobutylxanthine (Sigma, St. Louis, MO, USA), 1 μ g/mL Insulin (Novo Nordisk, Bagsvaerd, Denmark). After 4-days, differentiation medium was replaced with adipocyte maintenance medium (DMEM with 10% FBS and 1 μ g/mL Insulin), which was replaced every 2-days. For the cholesterol depletion experiments, after 10-days of differentiation, the adipocytes were washed with PBS and then incubated in medium supplemented with 10% delipidated FCS (J65182; Alfa Aesar, Tewksbury, MA, USA), 50 μ M sodium mevalonate (Sigma, St. Louis, MO), and 50 μ M sodium compactin (Sigma, St. Louis, MO) for 16-h. After this, the adipocytes were incubated in the same medium supplemented with either ethanol (vehicle control) or 1 μ g/ml cholesterol (Sigma) for 4-h. SREBP2 was detected with rabbit anti-SREBP2 (10007663; Cayman Chemical Company, Ann Arbor, MI, USA); SND1 was detected with rabbit anti-SND1 (4200470; Sigma); and actin was detected with mouse anti-actin (A1978; Sigma). The immunoblots were imaged and quantified with secondary antibodies and an Odyssey imaging system (LI-Biosciences, Lincoln, NE) as described⁵⁷ or a ChemiDoc™ MP imaging system Bio-RAD (Hercules, CA, USA) using Clarity Western ECL Substrate ECL (Cat # 170-5060; Bio-RAD). For the siRNA experiments, after 8-days of differentiation, the adipocytes were transfected with equivalent amounts of control (scrambled), mouse *Snd1* SMARTpool siRNA (56463; Dharmacon, Lafayette, CO), or mouse *Srebp2* SMARTpool siRNA (L-050073-01; Dharmacon) using Lipofectamine RNAiMAX (Thermo Fisher Scientific) according to the manufacturer's instructions. For the SND1 TNF α experiment, after 48-h, the adipocytes were treated with 10 ng/mL tumor necrosis factor- α (TNF α) (R&D systems, Minneapolis, MN) for 4-h as indicated, and the adipocytes were harvested for mRNA analysis.

Collagenase digestion of adipose tissue. Perigonadal adipose tissue was immediately minced and incubated in 1 mg/mL type I collagenase in DMEM for 30-min at 37 °C with agitation. The adipose was centrifuged at 600g for 10-min and the floating adipocytes and stromal vascular fraction isolated. Actin was detected with mouse anti actin, and SND1 was detected with mouse anti-SND1 (SAB4200504 (Sigma).

Microarray. Total RNA from perigonadal fat was isolated with an RNeasy lipid tissue mini kit (74804, Qiagen, Hilden, Germany) using Qiazol™ (Qiagen) as the adipose tissue lysis reagent. The RNA concentration and integrity was then characterized with an Agilent Bioanalyzer and analyzed by affymetrix mouse exon 2.0 arrays, which measured exon expression of 41,346 transcripts, at the University of Kentucky microarray facility. Data analysis was performed with Partek software on RMA-normalized data that was log₂-transformed. Additional analysis was performed with NIH David and gene set enrichment analysis. The data discussed in this publication have been deposited in NCBI's Gene Expression Omnibus and are accessible through GEO Series accession number GSE87661 (<https://www.ncbi.nlm.nih.gov/geo/query/acc.cgi?acc=GSE87661>).

Gene expression. Gene expression was determined by real time reverse transcriptase polymerase chain reaction as previously described⁵⁸. Standard curves were made from a pool of the cDNA, and gene expression was normalized to 18S. This allows for the measurement of relative changes in gene expression within the indicated experiment. The primer sequences are in Table 4.

Gene ^a	Forward primer	Reverse primer
<i>Snd1</i>	GGG ACG AGA GTA TGG GAT GAT	GCC TTC TGC AAC TAG CGA CT
<i>Ldlr</i>	AGT GGC CCC GAA TCA TTG AC	CTA ACT AAA CAC CAG ACA GAG GC
<i>Lss</i>	TCG TGG GGG ACC CTA TAA AAC	CGT CCT CCG CTT GAT AAT AAG TC
<i>Insig1</i>	TGT CGG TTT ACT GTA TCC CTG T	GTT GAT GCC AAC GAA CAC GG
<i>Lrrc4</i>	GAG GAG CTT GAG ATG TCA GGG	CCA GTC CGT CAA AAG CAT TCC
<i>Ccl19</i>	GGG GTG CTA ATG ATG CGG AA	CCT TAG TGT GGT GAA CAC AAC A
<i>Mcp1</i>	ACA CTG GTT CCT GAC TCC TCT	ATT AGA TTC GGT TTA ATT GGC CC
<i>Il6</i>	CCA AGA GGT GAG TGC TTC CC	CTG TTG TTC AGA CTC TCT CCC T
<i>Ccl19 e1</i>	CAC TCA CTC TCT GTG GCC TG	CAG AGA ACC AGC AGG CTG AA
<i>Ccl19 e2</i>	GAA GAC TGC TGC CTG TCT GT	ACC CTG CAG CCA TCT TCA TT
<i>Ccl19 e3</i>	GTT CAC CAC ACT AAG GGG CT	CTT CGG ATG ATG CGA TCC AC
<i>Ccl19 e4</i>	ATC ACT CTG GCC CAG GAA AC	CTT GGC TGG GTT AGG TCT GG
<i>Ccl19 e1-e4</i>	CAG TCA CTC CCC TGT GAA CC	CTT GGC TGG GTT AGG TCT GG
18S	GTAACCCGTTGAACCCATT	CCATCCAATCGGTAGTAGCG

Table 4. Primers. ^aThe sequences of primers used for realtime PCR are indicated. In addition, we designed primers to amplify the four exons of *Ccl19* (e1, e2, e3, and e4). The primers used to identify *Ccl19* isoforms (*Ccl19* e1–e4) by PCR in adipose tissue are also indicated.

Analysis of *Ccl19* splicing. For the analysis of *Ccl19* splicing in adipose tissue, cDNA was synthesized with QuantiTect Reverse Transcription Kit (Qiagen) from total RNA isolated from control and AdipoQ-LPL mice perigonadal adipose tissue. PCR was performed with above cDNA as template and primers located in exon 1 and exon 4 of *Ccl19* (Table 1). The PCR products were resolved in agarose gels, imaged and quantified with an Alphaimager HP system (proteinsimple, San Jose, CA, USA), isolated, and sequenced. For the analysis of *Ccl19* splicing in vitro, exon specific primers (Table 4) were used for realtime PCR on cDNA from control and SND1 siRNA transfected 3T3-L1 adipocytes with TNF α 4-h; mouse *Ccl19* plasmid DNA was used for the standard curve.

Energy metabolism studies. The study of mice in TSE calorimetry chambers was performed as described² except that the mice were studied on chow and then switched to a 60% high fat diet during the study. The indirect calorimetry data were analyzed by ANCOVA as previously described².

Mouse metabolic phenotyping. Glucose and insulin tolerance was performed as described². Insulin secretion was evaluated as follows. Blood (10 μ L) was isolated from the mouse tail vein at the indicated time after intraperitoneal glucose injection (10 days: 1 g/kg; 16 weeks: 2 g/kg) in a tube containing 1 μ L EDTA. Plasma insulin was measured using an ultrasensitive mouse insulin ELISA kit (#90080; Crystal Chem, IL) according to the manufacturer's instructions.

Statistical analysis. Data for the two groups of mice were analyzed by an unpaired, two-tailed student T-test. Multiple comparisons were analyzed by ANOVA and Tukey's post hoc analysis using Graph Pad Prism 5 and 7. Statistical significance was set at a P value less than 0.05.

Data availability

The datasets generated during and/or analyzed during the current study are available from the corresponding author on reasonable request.

Received: 25 May 2022; Accepted: 22 December 2022

Published online: 24 December 2022

References

- Wang, H. & Eckel, R. H. Lipoprotein lipase: From gene to obesity. *Am. J. Physiol. Endocrinol. Metab.* **297**, E271–288. <https://doi.org/10.1152/ajpendo.90920.2008> (2009).
- Walton, R. G. *et al.* Increasing adipocyte lipoprotein lipase improves glucose metabolism in high fat diet induced obesity. *J. Biol. Chem.* <https://doi.org/10.1074/jbc.M114.628487> (2015).
- Khan, T. *et al.* Metabolic dysregulation and adipose tissue fibrosis: Role of collagen VI. *Mol. Cell. Biol.* **29**, 1575–1591. <https://doi.org/10.1128/MCB.01300-08> (2009).
- Sun, K., Kusminski, C. M. & Scherer, P. E. Adipose tissue remodeling and obesity. *J. Clin. Invest.* **121**, 2094–2101. <https://doi.org/10.1172/JCI45887> (2011).
- Sun, K., Tordjman, J., Clement, K. & Scherer, P. E. Fibrosis and adipose tissue dysfunction. *Cell Metab.* **18**, 470–477. <https://doi.org/10.1016/j.cmet.2013.06.016> (2013).
- Le Lay, S. *et al.* Cholesterol, a cell size-dependent signal that regulates glucose metabolism and gene expression in adipocytes. *J. Biol. Chem.* **276**, 16904–16910. <https://doi.org/10.1074/jbc.M01095200> (2001).
- Ozcan, U. *et al.* Endoplasmic reticulum stress links obesity, insulin action, and type 2 diabetes. *Science* **306**, 457–461. <https://doi.org/10.1126/science.1103160> (2004).

8. da Huang, W., Sherman, B. T. & Lempicki, R. A. Systematic and integrative analysis of large gene lists using DAVID bioinformatics resources. *Nat. Protoc.* **4**, 44–57. <https://doi.org/10.1038/nprot.2008.211> (2009).
9. da Huang, W., Sherman, B. T. & Lempicki, R. A. Bioinformatics enrichment tools: Paths toward the comprehensive functional analysis of large gene lists. *Nucleic Acids Res.* **37**, 1–13. <https://doi.org/10.1093/nar/gkn923> (2009).
10. Beisiegel, U., Weber, W. & Bengtsson-Olivercrona, G. Lipoprotein lipase enhances the binding of chylomicrons to low density lipoprotein receptor-related protein. *Proc. Natl. Acad. Sci. USA* **88**, 8342–8346 (1991).
11. Bharadwaj, K. G. *et al.* Chylomicron- and VLDL-derived lipids enter the heart through different pathways: In vivo evidence for receptor- and non-receptor-mediated fatty acid uptake. *J. Biol. Chem.* **285**, 37976–37986. <https://doi.org/10.1074/jbc.M110.174458> (2010).
12. Goldberg, I. J., Eckel, R. H. & Abumrad, N. A. Regulation of fatty acid uptake into tissues: Lipoprotein lipase- and CD36-mediated pathways. *J. Lipid Res.* **50**(Suppl), S86–90. <https://doi.org/10.1194/jlr.R800085-JLR200> (2009).
13. Merkel, M. *et al.* Inactive lipoprotein lipase (LPL) alone increases selective cholesterol ester uptake in vivo, whereas in the presence of active LPL it also increases triglyceride hydrolysis and whole particle lipoprotein uptake. *J. Biol. Chem.* **277**, 7405–7411. <https://doi.org/10.1074/jbc.M107914200> (2002).
14. Merkel, M. *et al.* Catalytically inactive lipoprotein lipase expression in muscle of transgenic mice increases very low density lipoprotein uptake: Direct evidence that lipoprotein lipase bridging occurs in vivo. *Proc. Natl. Acad. Sci. USA* **95**, 13841–13846 (1998).
15. Obunike, J. C. *et al.* Cellular differences in lipoprotein lipase-mediated uptake of low density lipoproteins. *J. Biol. Chem.* **269**, 13129–13135 (1994).
16. Rumsey, S. C., Obunike, J. C., Arad, Y., Deckelbaum, R. J. & Goldberg, I. J. Lipoprotein lipase-mediated uptake and degradation of low density lipoproteins by fibroblasts and macrophages. *J. Clin. Investig.* **90**, 1504–1512. <https://doi.org/10.1172/JCI116018> (1992).
17. Mizuarai, S., Miki, S., Araki, H., Takahashi, K. & Kotani, H. Identification of dicarboxylate carrier Slc25a10 as malate transporter in de novo fatty acid synthesis. *J. Biol. Chem.* **280**, 32434–32441. <https://doi.org/10.1074/jbc.M503152200> (2005).
18. Subramanian, A. *et al.* Gene set enrichment analysis: A knowledge-based approach for interpreting genome-wide expression profiles. *Proc. Natl. Acad. Sci. USA* **102**, 15545–15550. <https://doi.org/10.1073/pnas.0506580102> (2005).
19. Mootha, V. K. *et al.* PGC-1 α -responsive genes involved in oxidative phosphorylation are coordinately downregulated in human diabetes. *Nat. Genet.* **34**, 267–273. <https://doi.org/10.1038/ng1180> (2003).
20. Liberzon, A. *et al.* The Molecular Signatures Database (MSigDB) hallmark gene set collection. *Cell Syst.* **1**, 417–425. <https://doi.org/10.1016/j.cels.2015.12.004> (2015).
21. Santhekadur, P. K. *et al.* Staphylococcal nuclease domain containing-1 (SND1) promotes migration and invasion via angiotensin II type 1 receptor (AT1R) and TGF β signaling. *FEBS Open Bio* **4**, 353–361. <https://doi.org/10.1016/j.fob.2014.03.012> (2014).
22. Santhekadur, P. K. *et al.* Multifunction protein staphylococcal nuclease domain containing 1 (SND1) promotes tumor angiogenesis in human hepatocellular carcinoma through novel pathway that involves nuclear factor kappaB and miR-221. *J. Biol. Chem.* **287**, 13952–13958. <https://doi.org/10.1074/jbc.M111.321646> (2012).
23. Yu, P., Ma, D. & Xu, M. Nested genes in the human genome. *Genomics* **86**, 414–422. <https://doi.org/10.1016/j.ygeno.2005.06.008> (2005).
24. Sano, T. *et al.* Protection from diet-induced obesity and insulin resistance in mice lacking CCL19-CCR7 signaling. *Obesity (Silver Spring)* **23**, 1460–1471. <https://doi.org/10.1002/oby.21127> (2015).
25. Duan, Z. *et al.* Tudor-SN, a novel coactivator of peroxisome proliferator-activated receptor gamma protein, is essential for adipogenesis. *J. Biol. Chem.* **289**, 8364–8374. <https://doi.org/10.1074/jbc.M113.523456> (2014).
26. Olefsky, J. M. & Glass, C. K. Macrophages, inflammation, and insulin resistance. *Annu. Rev. Physiol.* **72**, 219–246. <https://doi.org/10.1146/annurev-physiol-021909-135846> (2010).
27. Gregor, M. F. & Hotamisligil, G. S. Inflammatory mechanisms in obesity. *Annu. Rev. Immunol.* **29**, 415–445. <https://doi.org/10.1146/annurev-immunol-031210-101322> (2011).
28. Tourniaire, F. *et al.* Chemokine expression in inflamed adipose tissue is mainly mediated by NF- κ B. *PLoS One* **8**, 1. <https://doi.org/10.1371/journal.pone.0066515> (2013).
29. Cappellari, M. *et al.* The transcriptional co-activator SND1 is a novel regulator of alternative splicing in prostate cancer cells. *Oncogene* **33**, 3794–3802. <https://doi.org/10.1038/nc.2013.360> (2014).
30. Walton, R. G. *et al.* Increasing adipocyte lipoprotein lipase improves glucose metabolism in high fat diet-induced obesity. *J. Biol. Chem.* **290**, 11547–11556. <https://doi.org/10.1074/jbc.M114.628487> (2015).
31. Kojima, H. *et al.* Extraprostatic insulin-producing cells in multiple organs in diabetes. *Proc. Natl. Acad. Sci. USA* **101**, 2458–2463 (2004).
32. Chen, X., Larson, C. S., West, J., Zhang, X. & Kaufman, D. B. In vivo detection of extrapancreatic insulin gene expression in diabetic mice by bioluminescence imaging. *PLoS One* **5**, 9397. <https://doi.org/10.1371/journal.pone.0009397> (2010).
33. Le Lay, S., Ferre, P. & Dugail, I. Adipocyte cholesterol balance in obesity. *Biochem. Soc. Trans.* **32**, 103–106 (2004).
34. Boizard, M. *et al.* Obesity-related overexpression of fatty-acid synthase gene in adipose tissue involves sterol regulatory element-binding protein transcription factors. *J. Biol. Chem.* **273**, 29164–29171 (1998).
35. Xiao, H. *et al.* Sterol regulatory element binding protein 2 activation of NLRP3 inflammasome in endothelium mediates hemodynamic-induced atherosclerosis susceptibility. *Circulation* **128**, 632–642. <https://doi.org/10.1161/CIRCULATIONAHA.113.002714> (2013).
36. Armengol, S. *et al.* SREBP-2-driven transcriptional activation of human SND1 oncogene. *Oncotarget* **8**, 108181–108194. <https://doi.org/10.18632/oncotarget.22569> (2017).
37. Armengol, S. *et al.* The promoter of cell growth- and RNA protection-associated SND1 gene is activated by endoplasmic reticulum stress in human hepatoma cells. *BMC Biochem.* **15**, 25. <https://doi.org/10.1186/s12858-014-0025-2> (2014).
38. Armengol, S. *et al.* NF- κ B, Sp1 and NF-Y as transcriptional regulators of human SND1 gene. *Biochimie* **95**, 735–742. <https://doi.org/10.1016/j.biochi.2012.10.029> (2013).
39. Ochoa, B., Chico, Y. & Martinez, M. J. Insights into SND1 oncogene promoter regulation. *Front. Oncol.* **8**, 606. <https://doi.org/10.3389/fonc.2018.00606> (2018).
40. Jariwala, N. *et al.* Role of the staphylococcal nuclease and tudor domain containing 1 in oncogenesis (review). *Int. J. Oncol.* **46**, 465–473. <https://doi.org/10.3892/ijo.2014.2766> (2015).
41. Navarro-Imaz, H., Rueda, Y. & Fresnedo, O. SND1 overexpression deregulates cholesterol homeostasis in hepatocellular carcinoma. *Biochem. Biophys. Acta.* **988–996**, 2016. <https://doi.org/10.1016/j.bbali.2016.05.011> (1861).
42. Rajasekaran, D. *et al.* Staphylococcal nuclease and tudor domain containing 1 (SND1 protein) promotes hepatocarcinogenesis by inhibiting monoglyceride lipase (MGLL). *J. Biol. Chem.* **291**, 10736–10746. <https://doi.org/10.1074/jbc.M116.715359> (2016).
43. Arretxe, E. *et al.* Profiling of promoter occupancy by the SND1 transcriptional coactivator identifies downstream glycerolipid metabolic genes involved in TNF α response in human hepatoma cells. *Nucleic Acids Res.* **43**, 10673–10688. <https://doi.org/10.1093/nar/gkv858> (2015).
44. Navarro-Imaz, H. *et al.* Molecular and cellular insights into the role of SND1 in lipid metabolism. *Biochim. Biophys. Acta Mol. Cell Biol. Lipids* **1865**, 158589. <https://doi.org/10.1016/j.bbali.2019.158589> (2020).

45. Palacios, L., Ochoa, B., Gomez-Lechon, M. J., Castell, J. V. & Fresnedo, O. Overexpression of SND p102, a rat homologue of p100 coactivator, promotes the secretion of lipoprotein phospholipids in primary hepatocytes. *Biochem. Biophys. Acta* **1761**, 698–708. <https://doi.org/10.1016/j.bbali.2006.05.005> (2006).
46. Jeon, T. I. & Osborne, T. F. SREBPs: Metabolic integrators in physiology and metabolism. *Trends Endocrinol. Metab.* **23**, 65–72. <https://doi.org/10.1016/j.tem.2011.10.004> (2012).
47. Im, S. S. *et al.* Linking lipid metabolism to the innate immune response in macrophages through sterol regulatory element binding protein-1a. *Cell Metab.* **13**, 540–549. <https://doi.org/10.1016/j.cmet.2011.04.001> (2011).
48. Hellmann, J. *et al.* CCR7 maintains nonresolving lymph node and adipose inflammation in obesity. *Diabetes* **65**, 2268–2281. <https://doi.org/10.2337/db15-1689> (2016).
49. Orr, J. S. *et al.* CC-chemokine receptor 7 (CCR7) deficiency alters adipose tissue leukocyte populations in mice. *Physiol. Rep.* <https://doi.org/10.14814/phy2.12971> (2016).
50. Mashima, H. *et al.* Betacellulin and activin A coordinately convert amylase-secreting pancreatic AR42J cells into insulin-secreting cells. *J. Clin. Invest.* **97**, 1647–1654. <https://doi.org/10.1172/JCI118591> (1996).
51. Korsman, P. & Renstrom, E. Insulin granule dynamics in pancreatic beta cells. *Diabetologia* **46**, 1029–1045. <https://doi.org/10.1007/s00125-003-1153-1> (2003).
52. Pappan, K. L. *et al.* Pancreatic beta-cell lipoprotein lipase independently regulates islet glucose metabolism and normal insulin secretion. *J. Biol. Chem.* **280**, 9023–9029. <https://doi.org/10.1074/jbc.M409706200> (2005).
53. Cruz, W. S., Kwon, G., Marshall, C. A., McDaniel, M. L. & Semenkovich, C. F. Glucose and insulin stimulate heparin-releasable lipoprotein lipase activity in mouse islets and INS-1 cells. A potential link between insulin resistance and beta-cell dysfunction. *J. Biol. Chem.* **276**, 12162–12168. <https://doi.org/10.1074/jbc.M010707200> (2001).
54. Marshall, B. A. *et al.* Relative hypoglycemia and hyperinsulinemia in mice with heterozygous lipoprotein lipase (LPL) deficiency. Islet LPL regulates insulin secretion. *J. Biol. Chem.* **274**, 27426–27432 (1999).
55. Stern, J. H., Rutkowski, J. M. & Scherer, P. E. Adiponectin, leptin, and fatty acids in the maintenance of metabolic homeostasis through adipose tissue crosstalk. *Cell Metab.* **23**, 770–784. <https://doi.org/10.1016/j.cmet.2016.04.011> (2016).
56. Gomez-Banoy, N. *et al.* Adipsin preserves beta cells in diabetic mice and associates with protection from type 2 diabetes in humans. *Nat. Med.* **25**, 1739–1747. <https://doi.org/10.1038/s41591-019-0610-4> (2019).
57. Finlin, B. S. *et al.* DHA reduces the atrophy-associated Fn14 protein in differentiated myotubes during coculture with macrophages. *J. Nutr. Biochem.* **23**, 885–891. <https://doi.org/10.1016/j.jnutbio.2011.04.013> (2012).
58. Finlin, B. S. *et al.* Regulation of thrombospondin-1 expression in alternatively activated macrophages and adipocytes: Role of cellular cross talk and omega-3 fatty acids. *J. Nutr. Biochem.* **24**, 1571–1579. <https://doi.org/10.1016/j.jnutbio.2013.01.007> (2013).

Acknowledgements

We would like to acknowledge the excellent technical assistance and mouse colony management of Randi Narkovic. We would also like to acknowledge Dr. Kuey Chen and Donna Wall of the University of Kentucky microarray facility. We thank Dr. Philipp Scherer for the adiponectin promoter used to construct the transgenic mouse. The research reported in this publication was supported by an Institutional Development Award (IDeA) from the National Institute of General Medical Sciences of the National Institutes of Health under Grant number P30 127211 (BSF), supported by the DRC at Washington University, Grant No. 5 P30 DK020579 (BSF), supported by DK039176 (PAK), and partially supported by CTSA Grant UL1TR001998.

Author contributions

H.M. and B.Z. conducted most of the experiments. S.L. conducted the GSEA analysis. W.K. analyzed the calorimetry experimental data. P.A.K. contributed to the writing of the manuscript and data analysis. B.S.F. conceived the idea for the project, interpreted the data, and wrote the manuscript.

Competing interests

The authors declare no competing interests.

Additional information

Supplementary Information The online version contains supplementary material available at <https://doi.org/10.1038/s41598-022-26995-1>.

Correspondence and requests for materials should be addressed to B.S.F.

Reprints and permissions information is available at www.nature.com/reprints.

Publisher's note Springer Nature remains neutral with regard to jurisdictional claims in published maps and institutional affiliations.



Open Access This article is licensed under a Creative Commons Attribution 4.0 International License, which permits use, sharing, adaptation, distribution and reproduction in any medium or format, as long as you give appropriate credit to the original author(s) and the source, provide a link to the Creative Commons licence, and indicate if changes were made. The images or other third party material in this article are included in the article's Creative Commons licence, unless indicated otherwise in a credit line to the material. If material is not included in the article's Creative Commons licence and your intended use is not permitted by statutory regulation or exceeds the permitted use, you will need to obtain permission directly from the copyright holder. To view a copy of this licence, visit <http://creativecommons.org/licenses/by/4.0/>.

© The Author(s) 2022